

2024-10

Mechanical computing with transmissive snapping of kirigami shells

Y. Yang, J. Feng, D.P. Holmes. 2024. "Mechanical Computing with Transmissive Snapping of Kirigami Shells" *Advanced Functional Materials*, Volume 34, Issue 40. <https://doi.org/10.1002/adfm.202403622>
<https://hdl.handle.net/2144/50735>

"Downloaded from OpenBU. Boston University's institutional repository."

Mechanical Computing with Transmissive Snapping of Kirigami Shells

Yi Yang¹, Jin Feng², Douglas P. Holmes^{3*}

¹John A. Paulson School of Engineering and Applied Sciences, Harvard University,
29 Oxford St, Cambridge, MA 02138, USA

²Department of Mechanical Engineering, Massachusetts Institute of Technology
33 Mass Ave, Cambridge, MA 02138, USA

³Department of Mechanical Engineering, Boston University
110 Cummington Mall, Boston, MA 02215, USA

*To whom correspondence should be addressed; E-mail: dpholmes@bu.edu.

Continuum shape-morphing structures with the capability to encode memory and execute logic operations have garnered significant interest for the development of mechanical systems with embodied intelligence and soft robots. Achieving the integration of memory and computing within a mechanical system necessitates building blocks that possess a range of tunable, metastable states. Prior efforts have been dedicated to constructing mechanical memory and logic through the exploitation of snapping-through instability in multistable structures. Typically, the creation of each logic gate demands a distinct structural design. Here, we present a unconventional design strategy that leverages a single design of kirigami architecture to perform and switch between multiple fundamental logic operations. By utilizing the kirigami architecture as the fundamental elements, we demonstrate mechanical signal trans-

mission and perform half-adder computations. We envision that this design strategy can be applied to a wide range of materials and structures and path a new avenue to reduce complexity on develop materials system with embodied intelligence.

Introduction

Biological systems and organisms depend on their body morphologies for functions such as sensing, moving, controlling, and learning. Inspired by nature, computation through physical body morphology (1–4) has opened a new paradigm for sensing and processing information through elastic deformation of materials (5–9). While computing through morphology is broadly defined (10, 11), here, we consider morphology to be the combination of geometry (i.e. shape) and materials (i.e. elasticity) of a continuum physical body. Unlike linkage based mechanical computing (12, 13), the use of shape-morphing soft materials and flexible structures in mechanical computing has emerged as a potential approach for creating distributed, low-power sensors, and actuators (14–17). In mechanical systems, information can be written and erased through reversible shape-shifting of multistable structures (15, 18). For example, elastic bistable structures possessing a double-well energy potential serve as a non-volatile binary mechanical memory unit (19, 20). One level-up from encoding memory is performing binary logic operations which is grounded in Boolean algebra (15, 21–23). By integrating multiple logic gates, binary computation can be performed (24).

Mechanical binary logic and computation through Boolean algebra harnesses bistability of elastic structures in which one stable state is defined as ‘1’, and the other state is defined as ‘0’. Switching between two stable states is usually achieved with snap-through instabilities (25), triggered by various external stimulus such as moisture (26), fluid pressure (27, 28), mechanical loading (21, 22, 29), and swelling (23). Despite the triggering stimulus, in general, a specific

structural configuration needs to be designed for a specific logic operation (21, 22), which could limit its potential to be miniaturized and integrated into more complex circuits and computing systems. To overcome such barriers, efforts towards reprogrammable logic operations (30) and in-memory mechanical computing (14) have been proposed. However, challenges in integrating into more complex circuits and achieving scalability for potential soft robotic applications remains. To leverage continuum morphology of elastic body and reduce structural complexity without losing scalability, in this work, we designed a single kirigami shell architecture to perform and switch between multiple logic operations, including NOT, XNOR, and the universal logic gate, NAND. We also integrated the three logic gates into a half-adder to perform basic binary computation.

A single slit cut in the center of a plastic film may bend out-of-plane under tensile load upon reaching a tensile threshold (31). The flat geometry of a rectangular sheet with a single slit in the center can be described by the length of the film (L), the length of the slit (c), and the engraving margins along longitudinal direction (b) and transverse direction (w), as shown in Fig. 1A. In the kirigami structure, the width of the slit is much smaller than the length. Here, the width of the slit is selected as $0.05c$. We then confine the bending deformation of the free edges by clamping with polymethyl methacrylate (PMMA) beams. To trigger an anti-symmetric buckling mode (32), two infinitesimal cylindrical curvatures κ_0 with opposite signs are introduced as global imperfections (See Experimental Section).

We stretch and hold the sheet with a PMMA frame at a fixed stretch Δ , which is larger than the critical buckling threshold, such that the kirigami sheet buckles out-of-plane to form an anti-symmetric structure (Fig. 1B). This structure is composed of two identical buckled shells connected by two beams at the opposite free edges. Similar to a bistable compressed beam (33, 34), each buckled shell also has two stable configurations. Switching between the stable configurations can be achieved through a snap-through instability. Since two buckled shells are connected

by a quasi-rigid beams whose bending rigidity is much larger than the shell, the snapping dynamics of the two shells are coupled. As demonstrated in Fig. 1B, the snap-through of the excited shell (brown color) from convex configuration (buckles upwards) to concave configuration (buckles downwards) leads to the reconfiguration of the responsive shell (green color) from concave to convex. Here, we consider the snap-through of the responsive shell induced by the snap-through of the excited shell as a transmissive snapping. Upon snapping of the two shells, the kirigami structure morphs from the anti-symmetric mode, referred to as Mode A, to the reflection symmetry configuration about its undeformed plane, referred to as Mode A'.

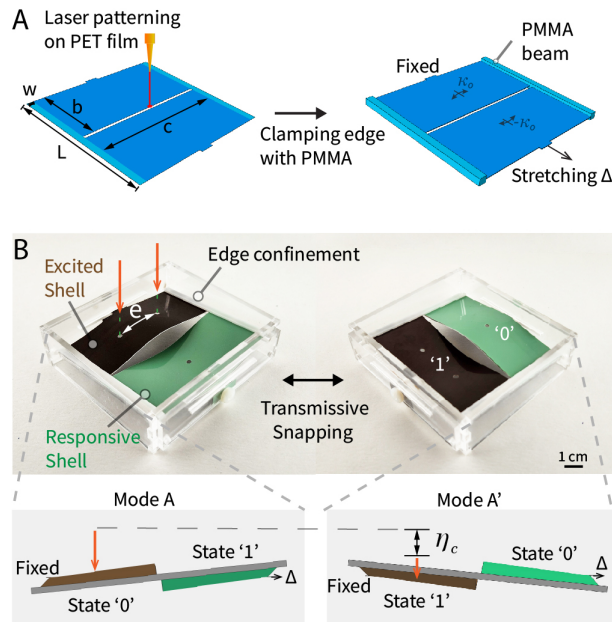


Figure 1: Edge confined multistable kirigami shell as a logic unit. (A) Schematics showing geometries and fabrication of the edge confined kirigami shell. (B) Reconfiguration of kirigami shell through a snap-through instability.

To describe the deformed states, we utilize the binary number and define the shell segment with a convex surface as state '0', and the shell with a concave surface as state '1'. In this way, information (0 1) is encoded in the system by pre-stretch. Logic operations are realized by

the transmissive snapping between the shells, i.e. the snap-through of the excited shell induces a snap-through of the responsive shell. NOT operation requires only a single input and output, respectively. Whereas, universal logic operation, e.g. NAND, requires two inputs and one output. In mechanical systems, mechanical indentation is commonly adopted as the input excitation signals. As shown in Fig. 1B, two indenters are placed evenly from the geometric center of the buckled shell with an eccentricity of $e/2$ along the laser cutting direction. By varying the critical indentation displacement required to trigger snapping (η_c) and the spacing between the two indenters (e), we gain the multifunctionality of both NAND and XNOR gate with this simple pre-stretched kirigami architecture. In the following sections, we will (i) investigate the transmissive snap-through instability as a function of the pre-stretch (Δ), (ii) obtain the spacing parameter between two indentation positions (e) to achieve universal logic operation, and (iii) incorporate the logic gates into an half-adder to perform fundamental binary mechanical computing.

Transmissive snap-through

To quantitatively investigate the snap-through behavior, we select the geometric parameters shown in Fig. 1A as, $c/w = 20$, $c/b = 2$, and $L \approx 2b$, where, $c = 76$ mm. We fabricated the kirigami shell using a plastic sheet (Artus Corporation) with a thickness of $h = 0.25$ mm and Young's modulus of $E = 4.33$ GPa, and clamped two free edges using polymethyl methacrylate (PMMA) beams with a thickness of 3.6 mm and Young's modulus of $E = 3.30$ GPa. As discussed previously, pre-stretch induced buckling gives the antisymmetric deformation mode of the kirigami shell. The amount of pre-stretch will change the elastic strain energy stored in the structure, which may affect the snap-through behavior upon indentation. To test our hypothesis, we arbitrarily select two distinct nominal strains, $\Delta = 0.8\%$ and $\Delta = 2.5\%$, as the pre-stretch. Displacement controlled indentation tests were performed quasi-statically on the

buckled kirigami shell using Instron 5940 at a rate of 0.2 mm/s. A single indenter is attached at the geometric center of the excited shell segment (See Figure S1 and Note S1 - Supporting Information).

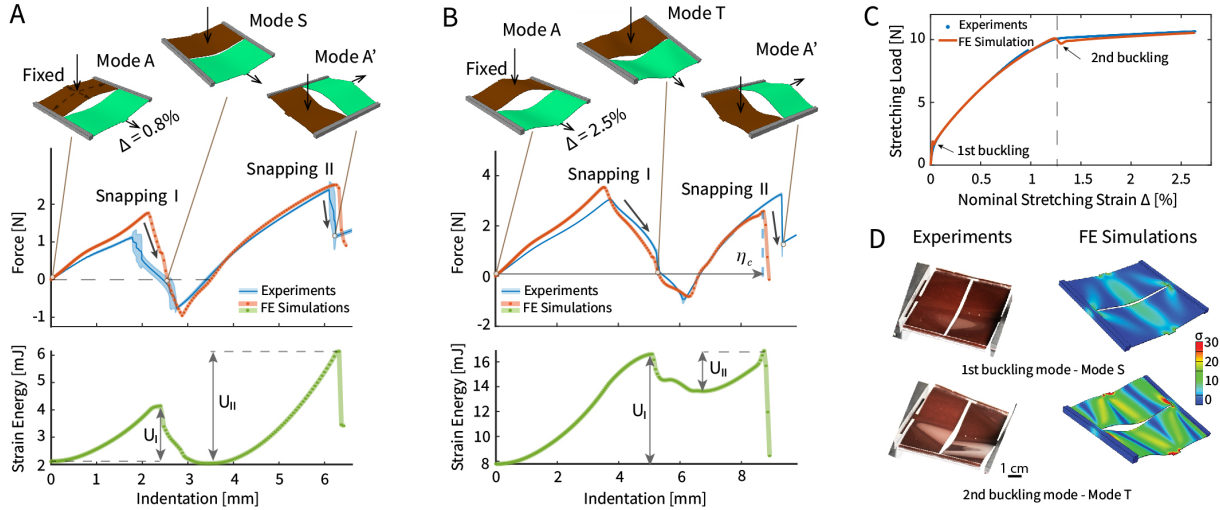


Figure 2: Mode transitions through transmissive snap-through. A-S-A' mode transitions (A) and A-T-A' mode transitions (B) triggered by mechanical indentation. (C) Effect of nominal stretching strain on the formation of the intermediate modes. (D) Intermediate modes as linear buckling eigenmodes. σ represents the Von Mises stress in MPa.

Interestingly, transitions from Mode A to Mode A' show sequential snap-through behavior with two snapping steps. This sequential snapping is a result of the quasi-rigid edge constraints. At the pre-stretch of 0.8% (Fig. 2A), the intermediate configuration deforms symmetrically which resembles the buckling of kirigami sheet with a single slit (31, 32). Here, this buckling mode is referred to as a slit mode (Mode S). To characterize the energy state of the system, we used finite element (FE) simulations to calculate the elastic strain energy of the two shell segments as a function of indentation during the mode transitions (See Note S2 - Supporting Information). In this way, we obtained the asymmetric energy landscape of the system and found the two energy barriers required to transition from Mode A to Mode S (U_I) and from

Mode S to Mode A' (U_{II}). Similarly, at the pre-stretch of 2.5% (Fig. 2B), transition from Mode A to Mode A' also requires an intermediate step. However, a distinct intermediate configuration is observed in which both shell segments twist as a twisted ribbon (35). This intermediate mode is referred to as a twisting mode (Mode T). Distinct from A-S-A' mode transition in which $U_I < U_{II}$, during A-T-A' mode transition, FE simulations show $U_I > U_{II}$. This observation may imply Mode S is an additional stable buckling mode with a lower energy state compared with Mode A, whereas, Mode T is another stable buckling mode with a higher energy state compared with Mode A, however, triggered by a different pre-stretch.

To test our hypothesis, we performed quasi-static uniaxial tensile tests on the kirigami shell before plastic yielding, experimentally and numerically (See Note S1, S2 - Supporting Information). Here, in order to obtain all possible buckling configurations, we removed the biased imperfection which triggers anti-symmetric deformation mode, and flattened the kirigami sheet ($\kappa_0 = 0$). Both experiment and FE simulation show two buckled configurations, Mode S and Mode T, as the pre-stretch increases (Fig. 2C). The buckling threshold and buckling mode are determined by the planar geometry of the sheet, h/c and b/c , (See Figure S2- Supporting Information). Fig. 2D shows the deformed configurations for Mode S and Mode T at a pre-stretch of 0.8 % and 2.5%, respectively. The strain energy calculated from FE simulation shows that Mode T is at a higher energy state compared with Mode S. We also performed linear buckling analysis using FE simulations to verify Mode S is the first buckling mode of the flat kirigami sheet under tensile loading, whereas, Mode T is the first buckling mode of the kirigami shell deforms in Mode S (See Note S2 - Supporting Information). Therefore, the intermediate state could have two buckling configurations (Mode S or Mode T) depending on the amount of pre-stretch. With a buckling threshold of $\Delta = 1.25\%$, secondary buckling occurs which introduces a mode transition from mode S to Mode T.

Kirigami Mechanical Logic

With the understanding on the mode formations and transitions due to pre-stretch, we leverage the sequential snap-through instability to perform binary logic operations in Boolean algebra. Here, we only utilize Mode S as the intermediate mode and keep the pre-stretch below the secondary buckling threshold. NOT operation generates a false output ('0') if the input is true ('1'). Therefore, mode transition from Mode A to Mode A' caused by single indentation acting on the excited shell (Fig. 2B) represents a NOT operation. To achieve functionally complete logic operations, e.g. NAND, two independent inputs are required to generate a single output. NAND gate generates a false output ('0') only if both inputs are true ('1'). To embed these logic operations in the kirigami shell, we exploit dual-point mechanical indentation to serve as two input signals. For the sake of simplicity, the two indenters are placed symmetrically about the longitudinal center line with a distance of e (Fig. 3A).

In our system, a single input signal is represented by a single-point indentation. Since the snap-through threshold of a pre-loaded structure is known to be position dependent and pre-load dependent (36, 37), the snapping threshold (η_c) to trigger mode transition from Mode A and Mode A' varies as a function of indentation position (e/c) and pre-stretch (Δ). Here, we denote the snapping threshold triggering mode transition with a single-point indentation and dual-point indentation are η_c^s and η_c^d , respectively. $\eta_c^s/\eta_c^d > 1$ indicates that by giving an fixed indentation displacement at $\eta = \eta_c^d$, dual-point indentation triggers the snapping but single-point indentation does not. By definition of NAND (Fig. 3B), $\eta_c^s/\eta_c^d > 1$ with an constrained indentation displacement at $\eta = \eta_c^d$ represents the NAND operation. Similarly, $\eta_c^s/\eta_c^d < 1$ indicates single-point indentation triggers the snapping at $\eta = \eta_c^s$ but dual-point indentation does not, which corresponds to an XNOR operation (Fig. 3B).

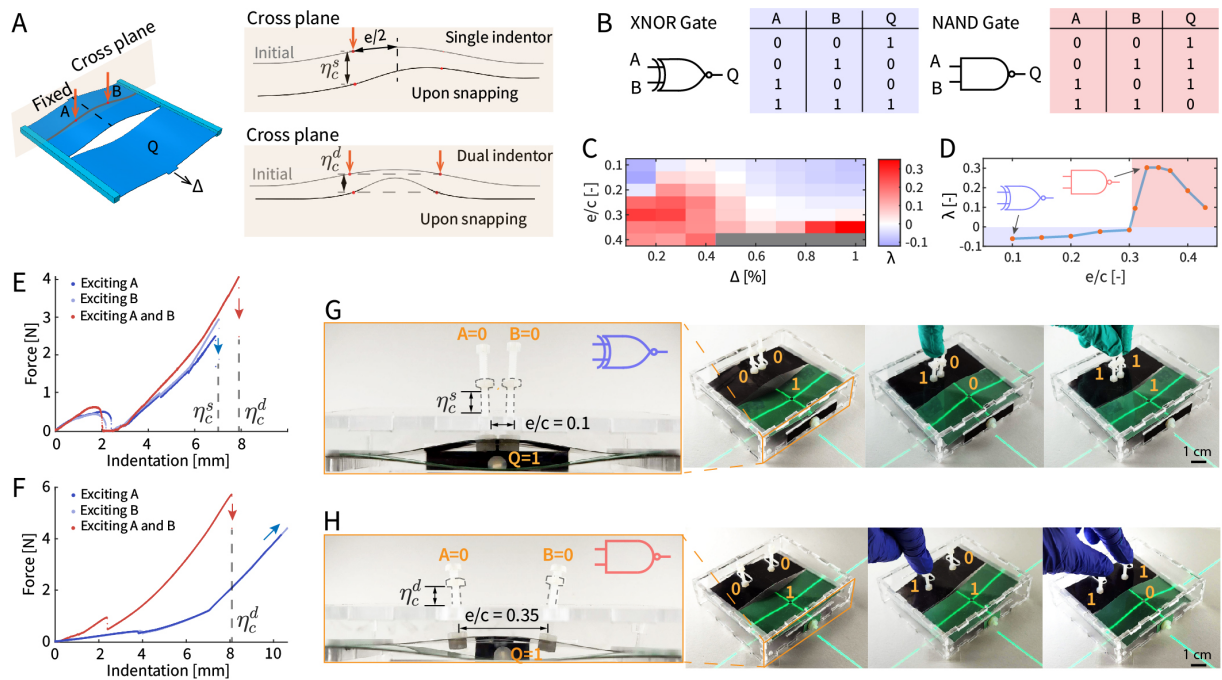


Figure 3: Kirigami mechanical logic gates. (A) Schematics illustrating single point and dual-point indentations. (B) Truth tables of XNOR gate and NAND gate. (C) FE simulation results showing $\lambda = 1 - \eta_c^s/\eta_c^d$ as a function of the indentation position (e/c) and the pre-stretching strain (Δ). Grey region indicates no snap-through observed. (D) FE results showing λ in terms of indentation position (e/c) at a constant pre-stretch, $\Delta = 0.8\%$. Experimental characterizations of the fabricated XNOR kirigami unit (E) and NAND kirigami unit (F). Demonstration of XNOR (G) and NAND (H) logic operations with a single kirigami architecture.

Here, we reformulate η_c^s/η_c^d as $\lambda = 1 - \eta_c^s/\eta_c^d$. Such that we can simply determine NAND and XNOR operation with $\lambda > 0$ and $\lambda < 0$, respectively. Our goal is to achieve both logic operations with a single kirigami architecture by altering two tunable parameters which impact the snapping threshold, pre-stretch (Δ) and indentation position (e/c). We employ FE simulations to quantitatively obtain λ as a function of e/c and Δ (See Note S3 - Supporting Information). As shown in Fig. 3C, we can achieve two logic operations by (i) tuning the pre-stretch from $\Delta = 0.14\%$ to $\Delta = 1.1\%$ at a fixed indentation position of $e/c = 0.25$, or (ii) varying indentation position from $e/c = 0.1$ to $e/c = 0.35$ with a constant pre-stretch of $\Delta = 0.84\%$. As we tune the pre-stretch and fix $e/c = 0.25$, the minimum λ we obtained is $\lambda = -0.06$ which corresponds to $e\eta_c^s - \eta_c^d = 0.39$ mm (See Supporting Data). As we vary the indentation position at a constant $\Delta = 0.84\%$, the minimum λ we obtained is $\lambda = 0.1$ which corresponds to $e\eta_c^s - \eta_c^d = 0.66$ mm. Limited by our fabrication technique, we choose to keep the pre-stretch at a constant of $\Delta = 1\%$, and vary e/c from 0.1 to 0.45 (Fig. 3D).

To realize logic operations, we fabricated two kirigami units for NAND and XNOR operations. The two units have identical kirigami architecture and the same amount of pre-stretch ($\Delta = 1\%$) applied by the PMMA frame. Guided by our FE simulations (Fig. 3D), we select the position parameter as $e/c = 0.1$ and $e/c = 0.35$ for XNOR gate and NAND gate, respectively. We characterized the sequential snapping behavior of the fabricated logic units experimentally through displacement-controlled mechanical indentation. The snapping behaviors of the two logic units agrees with our simulation. For the XNOR unit, single excitation of input portal A or B leads to $\eta_c^s = 6.9$ mm, whereas, dual excitation of both A and B yields $\eta_c^d = 7.8$ mm $> \eta_c^s$ (Fig. 3E). For NAND unit, single excitation causes large rotation of the unit about its longitudinal axis (stretching direction). Hence, second snapping is not observed even when the indentation reaches its preset limit at 10 mm. However, dual excitation of both input portals, A and B, gives $\eta_c^d = 8.2$ mm < 10 mm (Fig. 3F). Therefore, both fabricated kirigami architectures

operate as logic gates.

Control of pre-stretch and indentation (η_c^d, η_c^s) is realized by containing the kirigami logic unit in a PMMA box, as shown in Fig. 3G and H. The input portals are screws made with ABS plastics and are rigidly connected to the excited shell with bolts. The indentation depth can be simply adjusted by moving the nut along the screw. Here, we set $\eta_c^s = 7.5$ mm and $\eta_c^d = 8$ mm for XNOR gate and NAND gate, respectively. As demonstrated in Fig. 3G and H, the input portals are set as $A=B=0$ and the output is set to be $Q=1$ for both gates. Here, $Q=1$ is the default output value representing the concave configuration of the responsive shell. Two orthogonal laser sheets are shined on the output panel to illustrate snapping response. With a single true input ($A=1$) on the excited shell of the XNOR gate (Fig. 3G, See Movie - Supporting Information), the responsive shell will snap to a convex surface ($Q=0$) leading to mode reconfiguration from Mode A to Mode A'. But two true inputs ($A=B=1$) can only trigger the first snapping leading to transition from Mode A to Mode S. Whereas, to induce snapping of the responsive shell of the NAND gate (Fig. 3H, See Movie - Supporting Information), two true inputs ($A=B=1$) are required. Interestingly, employing the finger for indentation demonstrates that, even in the absence of precise vertical compression input, the kirigami logic unit can still effectively fulfill its intended function (See Movie - Supporting Information).

Kirigami Mechanical Computing

Universal logic gates are functionally complete set of logical connectives which can be integrated to higher-level combinational logic operations. To exemplify the potential applications of kirigami based mechanical computing, we combined NAND, XNOR, and NOT gates to construct a half adder. The architecture of the half adder and its truth table are illustrated in Fig. 4A. The half adder includes two input signals (A and B) and two output signals (Sum and Carry). The NAND gate and NOT gate are connected in series. In the same way, XNOR gate and NOT

gate are connected in series. Then, the two series of logic gates are connected in parallel.

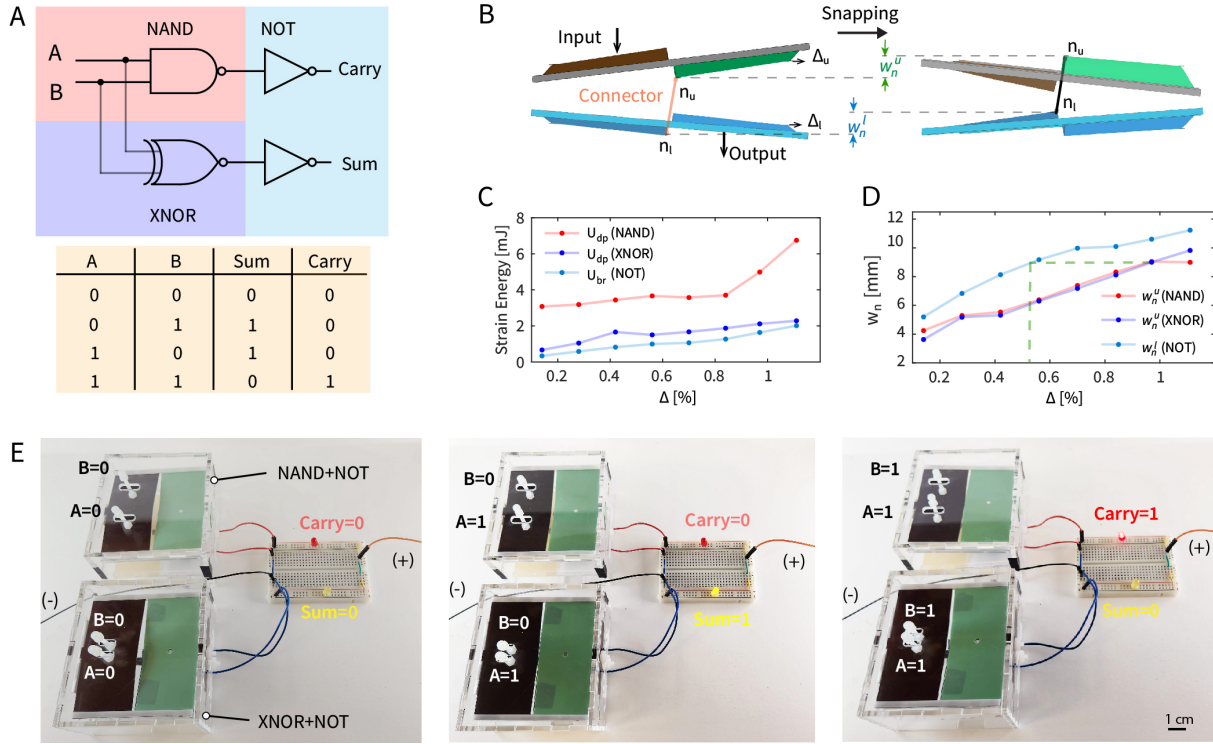


Figure 4: Kirigami mechanical computing. (A) Constructing half-adder with NAND, XNOR, and NOT gates. (B) Mechanical signal transmission between two kirigami units. (C) FE simulation results showing strain energy dissipation of NAND and XNOR gates and strain energy barrier of NOT gates upon snapping as a function of pre-stretch. (D) FE simulation results showing vertical displacement of the connecting nodes upon snapping in terms of pre-stretch. (E) Demonstration of half-adder operation. Scale bar represents 10 mm.

To realize the connection in series, we stacked two logic gates (Fig. 4B). NAND and XNOR gates are placed in the upper level, whereas NOT gates are placed in the lower level. Then, the input portals of the half adder, A and B, are connected to the excited shell of the NAND and XNOR gates. And the outputs, Sum and Carry, are connected to the responsive shells of the NOT gates. To transmit the snapping response from the upper unit to the lower unit, we employed a quasi-inextensible Nylon cable as a connector. The cable connects the responsive

shell of the upper unit to the excited shell of the lower unit at their center of the free edge marked as n_u to n_l for upper and lower unit in Fig. 4B, respectively. By given a pre-stretch for the upper unit (Δ_u) and lower unit (Δ_l), the cable is set to be almost straight but at a stress-free state. We assume the cable can only transfer tensile loading and will buckle like an elastica when being compressed. (See Figure S3 - Supporting Information for detailed construction of the half-adder)

In order to transfer the mechanical responses from the upper unit to the lower unit through snapping, we considered two criteria. First, the strain energy dissipation (U_{dp}) upon snapping for the upper unit is required to be higher than the energy barrier (U_{br}) triggering snapping of the lower unit from Mode S to Mode A', $U_{dp} > U_{br}$. Second, during mode transition from Mode A to Mode A', the total vertical displacement of the connected point of the upper unit, w_n^u , needs to be larger than the total vertical displacement of the connected point of the lower unit, w_n^l . In fact, strain energy dissipation, energy barrier, and vertical displacement all depend on the pre-stretch. From thin shell theory, where the deformation through shell thickness is ignored (32), strain energy is composed of bending energy ($U_b \sim Eh^3$) and membrane energy ($U_s \sim Eh$). Therefore, change of shell thickness will significantly affect the strain energy stored in the system, furthermore, change the strain energy dissipation and energy barrier. For the sake of simplicity, we keep the same material but select the thickness for the upper unit and lower unit as 0.25 mm and 0.2 mm, respectively.

In Fig. 4C, we calculated U_{dp} , U_{br} , w_n^u , and w_n^l in terms of the pre-stretch (Δ) using finite element simulations (See Figure S4 and S5 - Supporting Information). It is noted that larger Δ will change the intermediate configuration from Mode S to Mode T. Here, we set a limit of $\Delta=1.1\%$ for our simulations. All these terms grow monotonically as we increase the amount of the pre-stretch. For any given Δ , $U_{dp} > U_{br}$, and so our first criterion is satisfied automatically. In order to satisfy the second criterion, $w_n^u > w_n^l$, we may select $\Delta = 1\%$ for the upper unit

and $\Delta \leq 0.5\%$ for the lower unit. To visualize the snapping behaviors and signal transmission of the stacked logic gates, we build a simple electrical circuit with LED light and connected to the lower level unit (See Figure S3 - Supporting Information). Red LED is connected to the NAND+NOT unit, and the yellow LED is connected to the XNOR+NOT unit (Fig. 4D). Lighting of the red LED indicates a true output of the Carry (Carry=1). And lighting of the yellow LED indicates a true output of the Sum (Sum=1). Using the combination of universal kirigami logic gates, we performed a binary half adder as illustrated in Fig. 4D.

Conclusion and Discussion

In summary, we introduced an unconventional design strategy that employs the sequential snapping of a tristable kirigami shell for conducting universal logic operations and fundamental computing. The inherent characteristics of the tristable kirigami shell is a result of coupled snapping of two bistable buckled shells. In a binary mechanical logic system, ‘0’ and ‘1’ are encoded in a bistable element, e.g. shells and beams (19, 21, 22). These bistable elements are interconnected in different forms to create various logic gates. In this work, the presence of an additional intermediate stable state within the kirigami unit allows for an indirect transition from ‘0’ to ‘1’. This feature enables the implementation of three fundamental logic operations (NOT, XNOR, and NAND) using a single tristable kirigami shell, effectively minimizing the required number of building blocks for higher-level computations. In addition, we showcase the construction of a half-adder by stacking these three logic gates.

Apart from employing a single tristable kirigami shell for the execution of multiple binary logic operations, this platform could also serve as a means to independently carry out ternary logic operations. With three states (-1,0,+1) instead of two (1,0), ternary logic, which cannot be achieved with bistable structural elements (29, 38), has the inherent capacity to convey more information compared to binary logic. In ternary logic, we can define the modes A, S, and A’ as

‘-1’, ‘0’, ‘+1’, respectively. Snap-through instability in continuum structures, such as beams and shells, can be triggered by multiple numbers of inputs. In binary logic operations, either a single input or two inputs are sufficient to produce an output. Nevertheless, owing to the continuum shape morphing, this design platform has the potential to be extended to accommodate ternary logic operations, which may require three inputs. Due to the materials and scale independence of the transmissive snapping mechanism in the kirigami shell, we expect that this platform based on kirigami shell could unlock numerous possibilities for advancing mechanical computing and even contribute to the progression of developing materials with embodied intelligence.

Experimental Section

The plastic sheets are purchased from Artus Corporation, NJ. Plastic sheets with a thickness of 0.25 mm and 0.2 mm are used in the experiments. The Young’s modulus of the film is approximately 4.3 GPa and the Poisson’s ratio is 0.38. The kirigami pattern is cut with a laser cutter (Epilog Legend Helix laser machine) on the plastic sheets. Then, two PMMA (McMaster-Carr) beams are glued on the two free edges of the kirigami sheet with super glue (Loctite 403). For samples with infinitesimal curvature, excited shell and responsive shell are fabricated separately. Each shell is cut from plastic shim and mounted onto a steel bar with desired radius and placed in oven at 80 degree Celsius for 30 min. Then, two shells are glued together with the PMMA beams at the free edge by super glue. See Supporting Information for details on experiments and FE simulations.

References

1. K. Roy, A. Jaiswal, P. Panda, *Nature* **575**, 607 (2019).
2. V. C. Müller, M. Hoffmann, *Artificial Life* **23**, 1 (2017).

3. C. Laschi, B. Mazzolai, *IEEE Robotics & Automation Magazine* **23**, 107 (2016).
4. H. Hauser, A. J. Ijspeert, R. M. Fuchslin, R. Pfeifer, W. Maass, *Biological Cybernetics* **105**, 355 (2011).
5. E. Lejeune, P. Prachaseree, *Extreme Mechanics Letters* **63**, 102042 (2023).
6. M. Sitti, *Extreme Mechanics Letters* **46**, 101340 (2021).
7. R. L. Truby, *Accounts of Materials Research* **2**, 854 (2021).
8. C. Kaspar, B. J. Ravoo, W. G. van der Wiel, S. V. Wegner, W. H. P. Pernice, *Nature* **594**, 345 (2021).
9. M. A. McEvoy, N. Correll, *Science* **347** (2015).
10. R. M. Fuchslin, *et al.*, *Artificial Life* **19**, 9 (2013).
11. C. Paul, *Robotics and Autonomous Systems* **54**, 619 (2006).
12. R. C. Merkle, *et al.*, *Journal of Mechanisms and Robotics* **10** (2018).
13. M. M. Plecnik, J. Michael McCarthy, *Journal of Mechanisms and Robotics* **6** (2014). 031012.
14. T. Mei, C. Q. Chen, *Nature Communications* **14**, 5204 (2023).
15. H. Yasuda, *et al.*, *Nature* **598**, 39 (2021).
16. M. Garrad, G. Soter, A. T. Conn, H. Hauser, J. Rossiter, *Science Robotics* **4** (2019).
17. K. Nakajima, H. Hauser, T. Li, R. Pfeifer, *Scientific Reports* **5**, 10487 (2015).

18. H. Bense, M. van Hecke, *Proceedings of the National Academy of Sciences* **118**, e2111436118 (2021).
19. T. Chen, M. Pauly, P. M. Reis, *Nature* **589**, 386 (2021).
20. H. Yasuda, T. Tachi, M. Lee, J. Yang, *Nature Communications* **8**, 962 (2017).
21. Z. Meng, *et al.*, *Extreme Mechanics Letters* **43**, 101180 (2021).
22. Y. Song, *et al.*, *Nature Communications* **10**, 882 (2019).
23. Y. Jiang, L. M. Korpas, J. R. Raney, *Nature Communications* **10**, 128 (2019).
24. C. El Helou, B. Grossmann, C. E. Tabor, P. R. Buskohl, R. L. Harne, *Nature* **608**, 699 (2022).
25. D. P. Holmes, *Current Opinion in Colloid & Interface Science* **40**, 118 (2019).
26. B. Treml, A. Gillman, P. Buskohl, R. Vaia, *Proceedings of the National Academy of Sciences* **115**, 6916 (2018).
27. D. J. Preston, *et al.*, *Proceedings of the National Academy of Sciences* **116**, 7750 (2019).
28. J. A. Weaver, J. Melin, D. Stark, S. R. Quake, M. A. Horowitz, *Nature Physics* **6**, 218 (2010).
29. J. R. Raney, *et al.*, *Proceedings of the National Academy of Sciences* **113**, 9722 (2016).
30. T. Mei, Z. Meng, K. Zhao, C. Q. Chen, *Nature Communications* **12**, 7234 (2021).
31. M. A. Dias, *et al.*, *Soft Matter* **13**, 9087 (2017).
32. Y. Yang, M. A. Dias, D. P. Holmes, *Phys. Rev. Materials* **2**, 110601 (2018).

33. R. H. Plaut, *International Journal of Solids and Structures* **63**, 109 (2015).
34. A. Pandey, D. E. Moulton, D. Vella, D. P. Holmes, *EPL (Europhysics Letters)* **105**, 24001 (2014).
35. J. Chopin, A. Kudrolli, *Science Advances* **8**, eabi8818 (2022).
36. A. Fargette, S. Neukirch, A. Antkowiak, *Physical Review Letters* **112**, 137802 (2014).
37. J. Thompson, G. Hunt, *International Journal of Solids and Structures* **19**, 445 (1983).
38. H. Zhang, J. Wu, D. Fang, Y. Zhang, *Science Advances* **7**, eabf1966 (2021).

Supporting Information

Supporting Information is available online or from the authors.

Acknowledgments

The authors gratefully acknowledge the financial support from NSF through CMMI-1824882.